Type IX secretion system PorM and gliding machinery GldM form extended arches spanning the periplasmic space

Philippe Leone, Jennifer Roche, Maxence Vincent, Quang Hieu Tran, Aline Desmyter, Eric Cascales, Christine Kellenberger, Christian Cambillau, Alain Roussel

Type IX secretion system PorM and gliding machinery GldM form extended arches spanning the periplasmic space.

Philippe Leone[1,2,§], Jennifer Roche[1,2,§], Maxence S. Vincent[3], Quang Hieu Tran[1,2], Aline Desmyter[1,2], Eric Cascales[3], Christine Kellenberger[1,2], Christian Cambillau[1,2]* and Alain Roussel[1,2,]*

[1]Aix-Marseille Université, Architecture et Fonction des Macromolécules Biologiques, UMR 7257, Marseille, France.
[2]Centre National de la Recherche Scientifique, Architecture et Fonction des Macromolécules Biologiques, UMR 7257, Marseille, France.
[3] Laboratoire d'Ingénierie des Systèmes Macromoléculaires, Institut de Microbiologie de la Méditerranée, Aix-Marseille Université - Centre National de la Recherche Scientifique (UMR7255), 31 Chemin Joseph Aiguier, 13402 Marseille Cedex 20, France.

*Correspondence should be addressed to CC (cambillau@afmb.univ-mrs.fr) or AR (alain.roussel@afmb.univ-mrs.fr)

[§]These authors contributed equally to this work.

Running title: GldM and PorM crystal structures

The recently discovered type IX secretion system (T9SS), exclusively present in the *Bacteroidetes* phylum[1-4], has been studied mainly in *Flavobacterium johnsoniae* and *Porphyromonas gingivali*s. Among the 18 genes essential for complete T9SS function[5] a group of four, *porK-N* (*P. gingivalis*) or *gldK-M* (*F. johnsoniae*)[6] belongs to a co-transcribed operon[7] that expresses the T9SS core membrane complex[1]. The central component of this complex, PorM (or GldM), is anchored in the inner membrane (IM) by a trans-membrane helix and interacts through the outer membrane (OM) PorK-N complex[7]. Aside from genetic, biophysical and biochemical data, there is a complete lack of available atomic structures for any component of T9SS, including the PorKLMN complex. In this study, we report the three-dimensional crystal structure of the GldM and PorM periplasmic domains. GldM and PorM each contain four domains of ~180-Å length that span most of the periplasmic space. These and previously reported results make it possible to propose a model of the T9SS core membrane complex as well as its functional behaviour.

Bacteria, especially Gram-negative species, have assembled and evolved complex and specific cellular machines, known as secretion systems, to secrete proteins or DNA through the cell envelope into the surrounding medium or inside other cells[8]. In diderm bacteria, protein secretion occurs either as a one-step process, in which substrates are translocated directly from the cytoplasm to the external milieu, or as a two-step process, in which the substrates first cross the inner membrane (IM) into the periplasm using the Sec, Tat or holins pathways and then cross the outer membrane (OM) through a specialized translocon[8]. After secretion, the substrates might stay attached to the OM surface, be released into the extracellular milieu, or be injected into a target cell[8]. The type IX secretion system (T9SS) uses a two-step process. Depending of the bacterial strain, the T9SS confers very distinct functions. In *F. johnsoniae*, the T9SS contributes to gliding motility by secreting SprB, a cell surface adhesin that is required for movement on solid surfaces[9]. *P. gingivalis*, a non-motile bacterium, is a human oral pathogen and a major causative agent of periodontitis, as its T9SS secretes potent proteolytic enzymes called gingipains[10] that degrade host cell tissues and interfere with innate host defence mechanisms[11]. To date, 18 genes have been identified as essential for T9SS function in *P. gingivalis*[5]. Among them are a group of five genes, *porP-porK-porL-porM-porN*, which belong to a co-transcribed operon[7]. The last four genes have orthologues in the *F. johnsoniae* genome, *gldK-gldL-gldM-gldN*[6]. PorK, PorL, PorM and PorN, assemble as a > 1.4 MDa trans-membrane complex[1]. PorK (or GldK) is a lipoprotein

anchored to the OM that interacts with the periplasmic protein PorN[7,12]. PorL and PorM (GldL and GldM) are IM proteins that interact via their trans-membrane segments. The core of PorL resides in the cytoplasm, whereas PorM, similar to GldM, has a long periplasmic domain[7]. PorM interacts with both PorK and PorN complex, and therefore spans the entire periplasm by being anchored in the IM and interacting with the OM complex[7]. PorM (or GldM) is therefore a central structural component of the T9SS and an interesting target for structure and function studies. Here, we present the atomic structures of the periplasmic domains of both PorM and GldM, and provide information regarding the contribution of each domain for interaction with PorK and PorN.

The GldM (accession number GI: 58531935) and PorM periplasmic domains (GI: 188595218) (GldMp, PorMp) were cloned from residues 36-513 and 36-516, respectively. GldMp crystallized readily, and its structure was solved using the Se edge of a SeMet derivative for phasing (Supplementary Table 1). One molecule was present in the asymmetric unit, but strong contacts exist with a symmetry-related protein in the crystal. The assembly of GldMp as a dimer was confirmed because domain swapping and tight locking to the symmetry-related dimer were observed, which have been previously demonstrated for GldM in solution, as assessed by size exclusion chromatography (SEC).

The GldMp dimer is elongated and straight with overall dimensions of ~180 Å × 50 Å × 35 Å (Fig. 1). The dimer structure contains four domains, D1-D4 (Fig. 1) with seven α-helices and 22 β-strands in the sequence (α1−α2−α3−α4−α5) - (β1−β2−β3−β4−β5−β6) - (β7−β8−β9−β10−β11−β12−β13−β14) - (β15−β16−α6−β17−β18−β19−α7−β20−β21−β22).

Domain D1 (32-232) is formed by helices 1-5 in an up and down fold. The D1 domain dimers are packed together through helices α1. The D2 (233-320) and D3 (321-405) domains are exclusively formed of β-strands. Each D2 domain swaps its β-strands 1 and 2 with the other D2 domain, whereas D3 domains swap β-strand 7. The main plane of domain D3 is perpendicular to that of domain D2 (Fig. 1). The D4 domains (406-513) are not subject to domain swapping but are packed together in the dimer (Supplementary Table 2). The junctions between domains D1-D2 and D3-D4 are compact and thus prevent flexibility (Fig. 1 & Supplementary Fig. 1). However, the D2-D3 junctions are less compact and suggest that some bending may occur in solution. Remarkably, with a 180-Å extended conformation, GldM spans most of the periplasmic space, as the distances between the IM and OM associated with T3SS, T4SS and T6SS have been found to be ~260 Å[13], ~170 Å[14] and 180 Å[15], respectively.

The structural determination of PorMp was more tedious than that of GldMp. Full-length PorMp resisted all attempted crystallization assays. Trypsin cleavage experiments were therefore performed, and a defined fragment (residues 224-516, PorMp$_{224}$) was purified and crystallized[16] (Fig. 2a). Phasing was performed using Se-Met-substituted PorMp$_{224}$. Domains D2 and D3 could be traced fairly easily, but domain D4 was only partially constructed due to poor electron density map. In an attempt to stabilize this domain, we raised anti-PorMp llama antibodies and selected a nanobody (nb130) from the resulting library[17] that bound to PorMp with high affinity (K_D = 4.5 nM)[16]. We cloned a PorMp fragment between residues 224-516, co-crystallized it with nb130, and determined the structure of the complex (Fig. 2b). Surprisingly, the crystallized structure contained only domains D3 and D4, meaning that domain D2 was cleaved by a protease during crystallization; thus, the resulting structure spans residues 315-516 (PorMp$_{315}$). The D4 domain was easily traced in the electron density map because it was stabilized by nb130 binding, and it was introduced into the PorMp$_{224}$ structure, generating a complete model. The resulting PorMp$_{224}$ structure exhibits three domains that resemble GldMp domains D2-D4 (Fig. 1, 2b, 3). Interestingly, PorMp domains D2 and D3 possess a domain-swapping motif identical to that of GldMp (Fig. 3, Supplementary Fig. 2). Finally, we cloned, crystallized and determined the structure of the N-terminal domain of PorMp (residues 30-212) in complex with a nanobody (PorMp$_{Nt}$) (Fig. 2c; nanobody not represented).

Taken individually, the four domains of PorMp superimpose well with those of GldMp, with rmsd values ranging from 1.6 to 3.5 Å (Supplementary Table 3; Supplementary Fig. 2). Domains D3 and D4 of PorMp$_{224}$ and PorMp$_{315}$ share the same straight topology as those of GldM, whereas domain D2 is bent with respect to D3-D4 at an angle of ~45° because of the convolution of two rotations and a sliding of D3 monomers (Fig. 3; Supplementary Fig. 3).

Surprisingly, PorMp$_{Nt}$, the D1 domain of PorM, is missing the first helix (residues 30-69), which was probably cleaved during crystallization (Fig. 2c; Supplementary Fig. 2). Another difference between the D1 domains of GldMp and PorMp is the organization of dimer packing. In GldMp both D1 domains are packed side by side using their α1 helices; in PorMp$_{Nt}$, the four monomers in the asymmetric unit do not pack together, probably because the α1 helix that forms the D1 domain interface in GldMp is absent in this structure (Fig. 1). Finally, a complete domain can be modelled by assembling the various fragments using the GldMp scaffold: PorMp$_{315}$ was structurally aligned with PorMp$_{224}$, the PorMp$_{224}$ D2 domain was aligned with the GldMp D2 domain, and the PorMp$_{Nt}$ D1 domain was aligned with the

GldMp D1 domain, together with the modelling of the first PorMp$_{Nt}$ helix using α1 from GldMp D1 (Fig. 2d,e).

An interesting feature of both GldM and PorM is their D2-D3 domain-swapping motifs. To test whether this domain swapping exists *in vivo*, we first performed bacterial two-hybrid (BACTH) experiments. We found that the D2-D3 construct oligomerizes whereas the D1 and D4 isolated domains do not interact with themselves (Supplementary Fig. 4a). Based on the structure of PorMp, we introduced cysteine residues at different positions within the D2 and D3 domains of the full-length PorM protein (Supplementary Fig. 4b). SDS-PAGE analyses in absence of reducing agent demonstrated that residues Ala-318 from one monomer is at close distance from residue Ala-391 from the second monomer, whereas the Met-325 residues from two monomers face each other in the dimer (Supplementary Fig. 4c). These results confirm that the domain swapping occurs *in vivo*, in the context of the full-length protein.

The most striking difference observed between GldMp and PorMp is their overall topology, which results from the PorMp kink between D2 and D3 (Fig. 3, Supplementary Fig. 3). This kink is the result of two rotations around a vertical axis and around a horizontal axis, as in a cardan mount (Supplementary Fig. 3). Of note, the PorMp D2-D3 bending movement can occur in the left or the right direction, leading to two non-superimposable structures. The observation of bending in a unique direction suggests that the two forms may equilibrate by exchange through a transient straight form resembling GldMp. During crystallization, the equilibrium would be displaced towards the form accommodated in the crystal.

We previously reported that the periplasmic domain of PorM interacts with both PorK and PorN[7]. The contribution of PorM domains for contacting PorK and PorN was tested by BACTH. Our results show that the PorM D4 domain is sufficient for interacting with PorN. By contrast, PorM interaction with PorK requires the D2-D3 and D4 domains, suggesting that either the three domains are required for interaction or that D2-D3-mediated dimerization of the D4 domain (monomeric in the isolated form) is necessary to properly interact with PorK (Fig. 4a).

It has been reported by us[7] and others[1] that PorM binds to PorN. The K_D of the PorMp-PorN association, ~1 μM[7], is comparable to that of the association between the TssJ lipoprotein with TssM (K_D = 2-4 μM[18]), an event that initiates T6SS core complex assembly at the OM[15]. In turn, PorN binds to the PorK lipoprotein; therefore, the T9SS PorK-PorN complex might represent a functional equivalent of the T6SS TssJ lipoprotein, with equivalent binding

affinities for PorM or TssM. In the T6SS core complex, TssJ also binds the C-terminal D4 domain of TssM[15].

Sato *et al.*[1] isolated a core membrane complex of T9SS from *P. gingivalis* that was extracted using DDM. Analysis of this complex by western blot and SDS-PAGE revealed that it contains four components, PorK, PorL, PorM and PorN, and that its mass is slightly larger than 1.4 MDa[1]. We recently reported that PorM, PorL and PorK form homodimers, whereas PorL forms homotrimers[7]. Hence, the stoichiometry of the assembly is expected to be PorL$_3$/PorM$_2$/PorN$_2$-PorK$_2$, resulting in an overall mass of ~410 kDa. Therefore, three or four copies of the above-described assembly would be necessary to form the ~1.4 MDa isolated by Sato *et al.*[1].

In contrast, Gorasia *et al.* reported data that differ from those reported above[12]. In their report, a *P. gingivalis* membrane fraction was purified initially using DDM. Then, after switching to LDAO, they obtained large rings that were analysed with electron microscopy. These rings, which were attached to the membrane, measure ~50 nm in diameter (35 nm internally) and are formed of 32-36 1:1 PorK:PorN complexes. They did not observe the presence of PorM or PorL. These authors proposed that the native complex therefore contains 32 to 36 copies. The same rings were observed on the surface membrane of *P. gingivalis* mutants lacking *porL, porM and porP*. Strangely enough, despite the strong interaction measured between PorM and PorN, PorM was not observed in the complex. Furthermore, a pore of 350 Å would be very difficult to occlude during non-secretion periods. We therefore suspect that the gigantic pore reported in Gorasia *et al.* might be due to the absence of PorM/PorL in the preparations, resulting either from purification with LDAO or from the use of cells encoding a *porM* mutation. As often observed with protein-forming rings (e.g., phage portals[19], RAD52 or viral nucleocapsids), ring stoichiometry might vary in the absence of controlling elements.

Using the data from Sato *et al.*[1] and Vincent *et al.*[7], together with the structures reported here, we speculated on the possible architecture of the T9SS core machinery. We used Symmdock software[20] to identify which part of PorM/GldM might fit together to form a multimer of dimers. Using the straight GldMp structure, both 3-fold and 4-fold symmetry created associations involving mainly the D1 domain, and the rest of the structures exhibited a topology resembling that of tulip petals (Supplementary Fig. 5). This tulip shape is even more marked when PorMp is used, as its bending opens the D3-D4 arms to a larger degree. As a two-step secretion system, T9SS has to recruit effectors from the periplasm. To this end, the effectors must move through the PorM/GldM arches in a similar manner to how T2SS loads its cargo through the secretins[21,22].

By assembling all of the available data, we propose a schematic model of the T9SS core complex and secretion-associated opening based on the topology of the $PorL_3/PorM_2/PorN_2$-$PorK_2$ moieties (Fig. 4b,c). Each PorMp dimer is anchored in the IM by its two helices, which interact with the three helices of the PorL trimer. Close to the OM, the PorM D4 domain mediates contact with the PorN-PorK complex. The membrane-attached ring of $PorN_2/PorK_2$ should be associated with the secretion pore and may control its access by the effector. Interestingly, several possible candidates have been proposed controlling secretion, although no definitive arguments implicating a specific one have been made[3,5]. To note, Veith *et al.*[6] proposed that a cascade of several OM components might be associated with the core machinery for the post-treatment of effectors and their eventual association with the OM[6].

We speculate that the hinge between D2 and D3 may play a role in PorN/PorK opening, as it has been proposed that PorM is energized by the PorL trimer and that the two proteins form an energy transduction system for effector translocation[7,12,23]. The putative straight topology of PorM, resembling that of GldM, may therefore be associated with a closed state of the system. This state might be converted to the open form through a conformational change at the D2-D3 interface through PorL/PorM activation (Fig. 4b,c). Finally, we suggest that due to the structural similarity between PorM and GldM, both classical T9SS and Gld T9SS membrane core complexes might assemble and function in similar ways.

Materials and Methods

Protein production

The sequences corresponding to PorMp (residues 36-516), $PorMp_{315}$ (residues 224-516) and $PorMp_{Nt}$ (residues 44-217) were cloned into the pET28a+ derivative vector pLIC03, and the corresponding proteins, as well as selenomethionine-substituted (SeMet) PorMp, $PorMp_{224}$, and SeMet $PorMp_{224}$ were produced and purified as previously described[16,17]. The sequence corresponding to GldMp (residues 36-513) was amplified from *Flavobacterium johnsoniae* cDNA (ATCC17061, Leibniz Institute DSMZ) and was cloned into pLIC03 with the same protocol as for PorM constructs, using the primers 5'-CCGAGAACCTGTACTTCCAATCA*TTTGGTTTGATGAATGAAAAATTCG* and 5'-CGGAGCTCGAATTCGGATCCTTA*TTATTGTATTTCGTAAATTACCGG* (sequences annealing on the *porM* gene are italicized). GldMp and SeMet GldMp were produced in Rosetta *E. coli* cells and purified by nickel-affinity chromatography followed by size exclusion chromatography, with the same protocol as for PorM constructs.

Generation and purification of PorM-specific llama nanobodies.

The PorM specific nanonbodies nb01 and nb02 were selected and produced as previously described[17].The complexes PorMp$_{Nt}$/nb01 and PorMp$_{315}$/nb130 were purified as previously described [17].

Crystallization, data collection and processing

Crystallization, data collection and processing of PorMp$_{224}$, SeMet PorMp$_{224}$ and complexes PorMp$_{Nt}$/nb01 and PorMp$_{315}$/nb130 were performed as previously described[16,17]. Initial crystallization trials of GldMp and SeMet GldMp were performed by the sitting-drop vapour-diffusion method at 293K in 96-well Swissci plates using a Mosquito Crystal robot (TTP Labtech) with the following screens: Stura Footprint Screens (Molecular Dimensions), Structure Screen and Structure Screen 2 (Molecular Dimensions), PEGs Suite and PEGs II Suite (Qiagen), JCSG+ Suite (Qiagen), and Index (Hampton Research). Crystallization hit occurred in condition No. 8 of the Stura Footprint Screen #2 [0.1M Hepes pH7.5, 45%(w/v) PEG 600]. After optimization, the final crystallization conditions were 0.1M Hepes pH7.0-8.0, 26-46%(w/v) PEG 600. Crystals were briefly soaked in crystallization solution supplemented with 10% (v/v) ethylene glycol and 10% (v/v) glycerol for native and SeMet GldMp, respectively. Native GldMp diffraction data were collected to 2.0Å resolution on beamline ID30A-3 at the European Synchrotron Research Facility (ESRF), Grenoble, France. SeMet GldMp single-wavelength anomalous diffraction (SAD) data were collected to 2.4Å resolution on beamline Proxima-1 at SOLEIL, Paris, France. A fluorescence scan was performed to determine the peak wavelength (0.97908Å). The data sets were integrated with XDS [24] and were scaled with SCALA from CCP4 Suite [25]. Data collection statistics are reported in Supplementary Table 1.

Structure determination

The structure of PorMp$_{224}$ was solved by the multiple-wavelength anomalous diffraction (MAD) method using the SeMet PorMp$_{224}$ data set at 3.1Å resolution. Heavy-atom substructure determination, positional refinement, phase calculations and solvent flattening were performed using autoSHARP[26], SHARP [27] and SOLOMON [28], as previously described [16]. The partial model of SeMet PorMp$_{224}$ was built using Turbo-Frodo[29], and was

subsequently used as model for molecular replacement with MOLREP [30] to solve the structure of native PorMp$_{224}$ at 2.85Å.

The structure of the complex PorMp$_{315}$/nb130 was solved by molecular replacement with MOLREP [30] using the partial model of domains D3 and D4 of PorMp$_{224}$, and the structure of nb130 [17]as models. The building of domain D4 of PorMp$_{224}$ and PorMp$_{315}$ was then completed manually with COOT[31].

The structure of the complex PorMp$_{Nt}$/nb01 was solved by combining molecular replacement with MOLREP[30] using the structure of nb01 [17]as starting model, and several cycles of automatic building of PorMp$_{Nt}$ in the extra density with BUCCANEER[32]followed by refinement with autoBUSTER[33].The building of PorMp$_{Nt}$ was then completed manually with COOT[31].

The structure of GldMp was solved by the SAD method using the SeMet GldMp data set collected at 2.4Å. Heavy-atom substructure determination, positional refinement, phase calculations and solvent flattening were performed using autoSHARP [26], SHARP [27] and SOLOMON [28]. The partial model of SeMet GldMp was automatically built with BUCANEER[32], and was subsequently used as model for molecular replacement with MOLREP[30] to solve the structure of native GldMp at 2.0Å. The building of GldMp was then completed manually with COOT[31].

Refinement, correction and validation of the different structures were performed with autoBUSTER[33], COOT[31] and Molprobity[34], respectively. Refinement statistics are reported in Supplementary Table 1.

Bacterial two-hybrid (BACTH)

PorM-D1, PorM-D2-D3-D4, PorM-D2-D3 and PorM-D4 domains fused to the T18 and T25 domains of the *Bordetella* adenylate cyclase have been engineered by restriction-free ligation (oligonucleotide sequences available upon request). BACTH experiments have been performed as previously described[7].

In vivo disulphide bond formation.

Cysteine codons were introduced by Quick change site-directed mutagenesis into the plasmid encoding the C92S variant of FLAG-tagged PorM[7]. After gene induction, cells were lysed, and the total membrane fractions obtained after ultracentrifugation were subjected to 10%-acrylamide SDS-PAGE, transfer to nitrocellulose and immunodetection using monoclonal anti-FLAG antibody.

References

1   Sato, K. et al. A protein secretion system linked to bacteroidete gliding motility and pathogenesis. Proceedings of the National Academy of Sciences of the United States of America 107, 276-281, doi:10.1073/pnas.0912010107 (2010).

2   Sato, K. et al. Identification of Porphyromonas gingivalis proteins secreted by the Por secretion system. FEMS microbiology letters 338, 68-76, doi:10.1111/1574-6968.12028 (2013).

3   McBride, M. J. & Zhu, Y. Gliding motility and Por secretion system genes are widespread among members of the phylum bacteroidetes. Journal of bacteriology 195, 270-278, doi:10.1128/JB.01962-12 (2013).

4   Abby, S. S. et al. Identification of protein secretion systems in bacterial genomes. Sci Rep 6, 23080, doi:10.1038/srep23080 (2016).

5   Lasica, A. M., Ksiazek, M., Madej, M. & Potempa, J. The Type IX Secretion System (T9SS): Highlights and Recent Insights into Its Structure and Function. Frontiers in cellular and infection microbiology 7, 215, doi:10.3389/fcimb.2017.00215 (2017).

6   Veith, P. D., Glew, M. D., Gorasia, D. G. & Reynolds, E. C. Type IX secretion: the generation of bacterial cell surface coatings involved in virulence, gliding motility and the degradation of complex biopolymers. Molecular microbiology, doi:10.1111/mmi.13752 (2017).

7   Vincent, M. S. et al. Characterization of the Porphyromonas gingivalis Type IX Secretion Trans-envelope PorKLMNP Core Complex. The Journal of biological chemistry 292, 3252-3261, doi:10.1074/jbc.M116.765081 (2017).

8   Costa, T. R. et al. Secretion systems in Gram-negative bacteria: structural and mechanistic insights. Nature reviews. Microbiology 13, 343-359, doi:10.1038/nrmicro3456 (2015).

9   Nelson, S. S., Bollampalli, S. & McBride, M. J. SprB is a cell surface component of the Flavobacterium johnsoniae gliding motility machinery. Journal of bacteriology 190, 2851-2857, doi:10.1128/JB.01904-07 (2008).

10   Curtis, M. A. et al. Molecular genetics and nomenclature of proteases of Porphyromonas gingivalis. J Periodontal Res 34, 464-472 (1999).

11   Hajishengallis, G. Periodontitis: from microbial immune subversion to systemic inflammation. Nat Rev Immunol 15, 30-44, doi:10.1038/nri3785 (2015).

12   Gorasia, D. G. et al. Structural Insights into the PorK and PorN Components of the Porphyromonas gingivalis Type IX Secretion System. PLoS pathogens 12, e1005820, doi:10.1371/journal.ppat.1005820 (2016).

13   Nans, A., Kudryashev, M., Saibil, H. R. & Hayward, R. D. Structure of a bacterial type III secretion system in contact with a host membrane in situ. Nat Commun 6, 10114, doi:10.1038/ncomms10114 (2015).

14   Low, H. H. et al. Structure of a type IV secretion system. Nature 508, 550-553, doi:10.1038/nature13081 (2014).

15   Durand, E. et al. Biogenesis and structure of a type VI secretion membrane core complex. Nature 523, 555-560, doi:10.1038/nature14667 (2015).

16   Stathopulos, J., Cambillau, C., Cascales, E., Roussel, A. & Leone, P. Crystallization and preliminary X-ray analysis of the C-terminal fragment of PorM, a subunit of the Porphyromonas gingivalis type IX secretion system. Acta crystallographica. Section F, Structural biology communications 71, 71-74, doi:10.1107/S2053230X1402559X (2015).

17   Duhoo, Y. et al. Camelid nanobodies used as crystallization chaperones for different constructs of PorM, a component of the type IX secretion system from Porphyromonas gingivalis. Acta crystallographica. Section F, Structural biology communications 73, 286-293, doi:10.1107/S2053230X17005969 (2017).

18   Felisberto-Rodrigues, C. et al. Towards a structural comprehension of bacterial type VI secretion systems: characterization of the TssJ-TssM complex of an Escherichia coli pathovar. PLoS pathogens 7, e1002386, doi:10.1371/journal.ppat.1002386 (2011).

19   Lebedev, A. A. et al. Structural framework for DNA translocation via the viral portal protein. The EMBO journal 26, 1984-1994, doi:10.1038/sj.emboj.7601643 (2007).

20   Schneidman-Duhovny, D., Inbar, Y., Nussinov, R. & Wolfson, H. J. PatchDock and SymmDock: servers for rigid and symmetric docking. Nucleic acids research 33, W363-367, doi:10.1093/nar/gki481 (2005).

21   Douzi, B., Ball, G., Cambillau, C., Tegoni, M. & Voulhoux, R. Deciphering the Xcp Pseudomonas aeruginosa type II secretion machinery through multiple interactions with substrates. The Journal of biological chemistry 286, 40792-40801, doi:10.1074/jbc.M111.294843 (2011).

22   Korotkov, K. V., Sandkvist, M. & Hol, W. G. The type II secretion system: biogenesis, molecular architecture and mechanism. Nature reviews. Microbiology 10, 336-351, doi:10.1038/nrmicro2762 (2012).

23   Nakane, D., Sato, K., Wada, H., McBride, M. J. & Nakayama, K. Helical flow of surface protein required for bacterial gliding motility. Proceedings of the National Academy of Sciences of the United States of America 110, 11145-11150, doi:10.1073/pnas.1219753110 (2013).

24   Kabsch, W. Xds. Acta Crystallogr D Biol Crystallogr 66, 125-132, doi:S0907444909047337 (2010).

25   Winn, M. D. et al. Overview of the CCP4 suite and current developments. Acta Crystallogr D Biol Crystallogr 67, 235-242, doi:10.1107/S0907444910045749 (2011).

26   Vonrhein, C., Blanc, E., Roversi, P. & Bricogne, G. Automated structure solution with autoSHARP. Methods Mol Biol 364, 215-230, doi:10.1385/1-59745-266-1:215 (2007).

27   Bricogne, G., Vonrhein, C., Flensburg, C., Schiltz, M. & Paciorek, W. Generation, representation and flow of phase information in structure determination: recent developments in and around SHARP 2.0. Acta Crystallogr D Biol Crystallogr 59, 2023-2030 (2003).

28   Abrahams, J. P. & Leslie, A. G. Methods used in the structure determination of bovine mitochondrial F1 ATPase. Acta Crystallogr D Biol Crystallogr 52, 30-42, doi:10.1107/S0907444995008754 (1996).

29   Roussel, A., Cambillau, C. in in: Silicon Graphics Geometry Partners Directory 81 (Silicon Graphics Corp., 1991).

30   Vagin, A. & Teplyakov, A. Molecular replacement with MOLREP. Acta Crystallogr D Biol Crystallogr 66, 22-25, doi:10.1107/S0907444909042589 (2010).

31   Emsley, P. & Cowtan, K. Coot: model-building tools for molecular graphics. Acta Crystallogr D Biol Crystallogr 60, 2126-2132 (2004).

32   Cowtan, K. Completion of autobuilt protein models using a database of protein fragments. Acta Crystallogr D Biol Crystallogr 68, 328-335, doi:10.1107/S0907444911039655 (2012).

33   Blanc, E. et al. Refinement of severely incomplete structures with maximum likelihood in BUSTER-TNT. Acta Crystallogr D Biol Crystallogr 60, 2210-2221, doi:S0907444904016427 [pii]
10.1107/S0907444904016427 (2004).

34   Chen, V. B. et al. MolProbity: all-atom structure validation for macromolecular crystallography. Acta Crystallogr D Biol Crystallogr 66, 12-21, doi:10.1107/S0907444909042073 (2010).
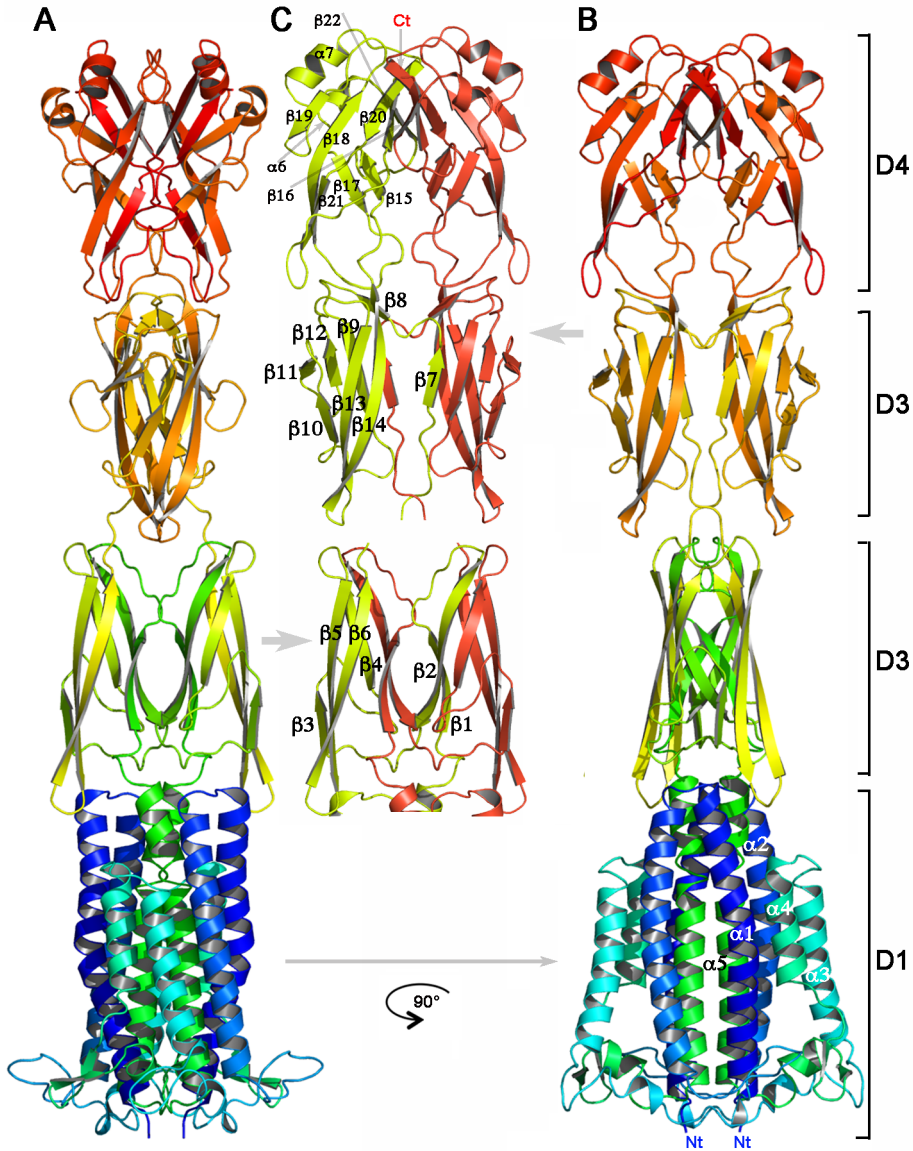
Figure legends

Figure 1: Crystal structure of GldMp from *Flavobacterium johnsoniae*. a, Ribbon view of the GldMp structure rainbow coloured from the N-terminus (blue) to the C-terminus (red). **b,** The same representation, 90° from (a). The four domains are labelled D1, D2, D3 and D4. **c,** Domains are coloured by polypeptide chain, yellow and red. Note the swapped β-strands in domains D2 (β1 and β2) and D3 (β7). Top, the secondary structure schematic.
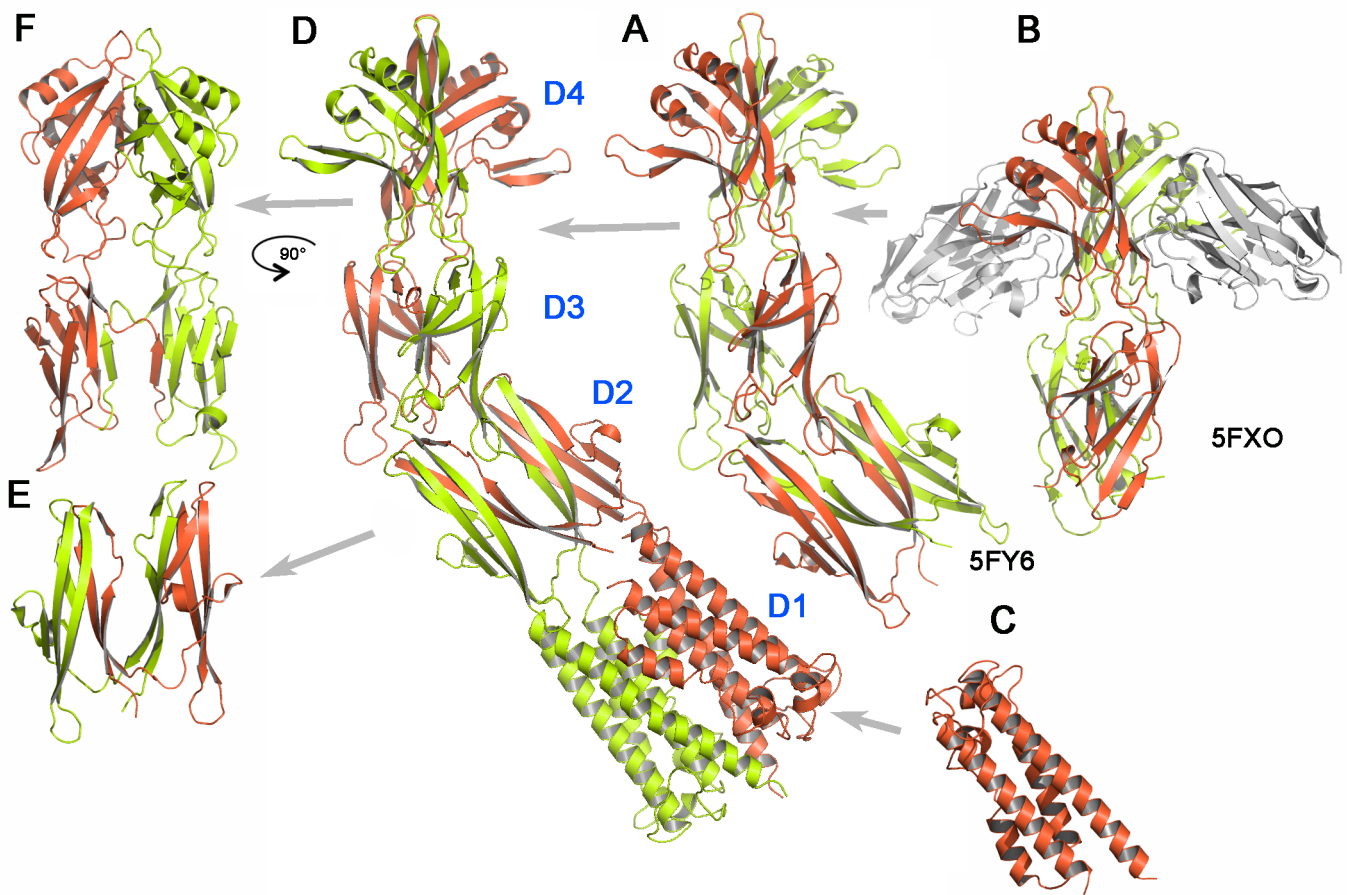
Figure 2: Crystal structure of PorMp from *Porphyromonas gingivalis*. a, Ribbon view of the $PorMp_{224}$ fragment structure (residues 224-516) and, **b,** of the $PorMp_{335}$ fragment structure (residues 224-516) in complex with the nanobody nb130 coloured by polypeptide chain (yellow and red, grey for nb130). **c,** Ribbon view of the $PorMp_{nt}$ fragment (nanobody not shown). **d**, Ribbon view of a PorMp model obtained by aligning the N-terminal D1 domain and the D2 domain on the GldMp scaffold. The domains are numbered D1-D4. **e,** The D2 domain rotated by 45°. **f**, 90° view of D3-D4 with respect to (d). **(a-f)** chains A and B are coloured green and red, respectively. Note the swapped β-strands in domains D2 (β1 and β2) and D3 (β7).
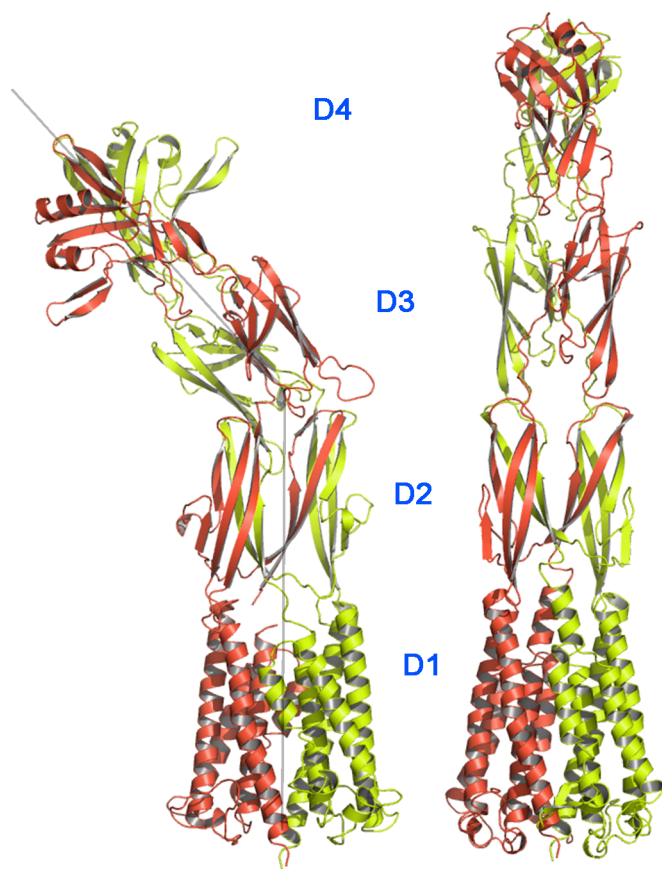
Figure 3: Comparison of GldMp and PorMp structures. Left, PorMp structure; right, GldMp structure (chain A and B are coloured in green and red, respectively). Both structures have been aligned using their D1 and D2 domains. Domains are numbered D1-D4 from their N- to C-termini. Note the ~45° angle between D1-D2 and D3-D4 PorMp domains.

Figure 4: Topological and functional models of PorM and GldM core membrane complexes. a, Bacterial two-hybrid analysis. BTH101 reporter cells carrying pairs of plasmids producing the indicated PorM fragments fused to T18, and PorK or PorN fused to T25 were spotted on X-Gal-IPTG reporter LB agar plates. The blue coloration of the colony reports interaction between the two partners. Controls include T18 and T25 fusions to TolB and Pal, two proteins that interact but unrelated to the T9SS. **b,** Representation of an "open" topology (during secretion) and, **c,** of a "closed" topology (system at rest). The model shows PorM as in the crystal structure (a) and extended as in the GldM structure (b). The rest of the model collects data from previous reports[1,6,7]. K, L, M, and N schematically represent PorK, L, M, and N or GldK, L, M, and N.
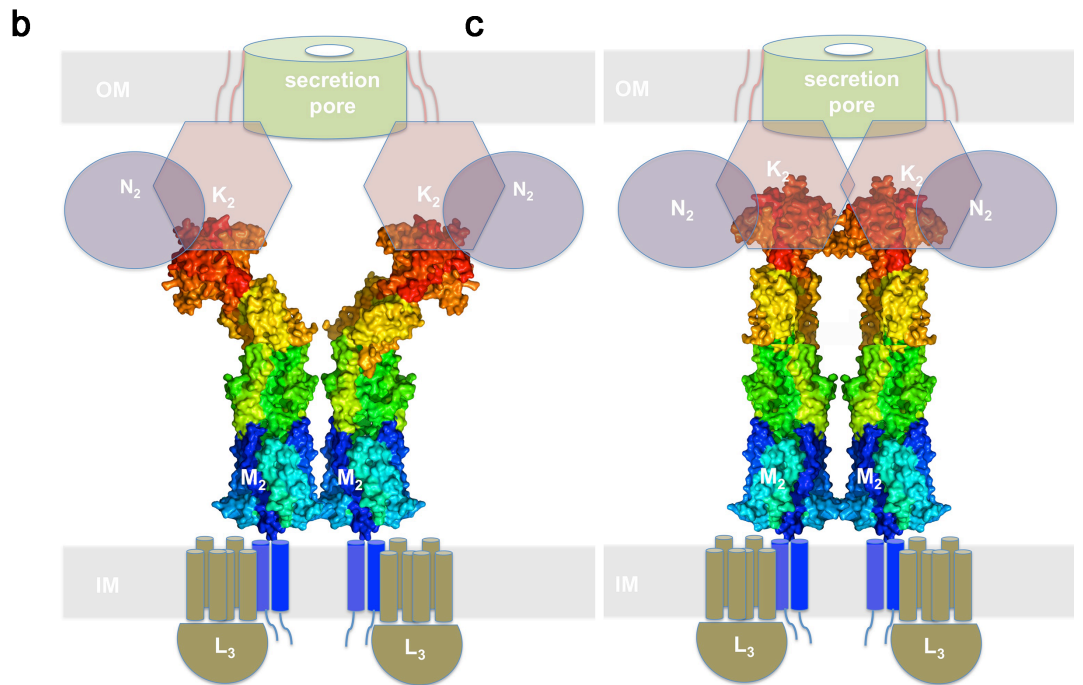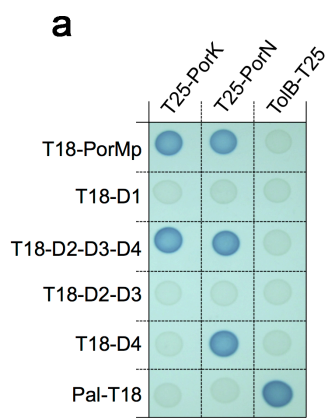
(α1-α2-α3-α4-α5)–(β1-β2-β3-β4-β5-β6)–(β7-β8-β9-β10-β11-β12-β13-β14)–(β15-β16-α6-β17-β18-β19-α7-β20-β21-β22)

D1   D2   D3   D4

A   C   Ct   B

β22

α7   β20

β19   β18

α6

β16   β17   β15   D4

β21

β8

β12   β9

β11   β7

β13

β10   β14   D3

D3

β5 β6

β4   β2

β3   β1   D3

α2

α4

α1

α5   α3   D1

Nt   Nt

D4

D3

D2

D1

Type IX secretion system PorM and gliding machinery GldM form extended arches spanning the periplasmic space.

Philippe Leone[1,2,§], Jennifer Roche[1,2,§], Maxence S. Vincent[3], Quang Hieu Tran[1,2], Aline Desmyter[1,2], Eric Cascales[3], Christine Kellenberger[1,2], Christian Cambillau[1,2]* and Alain Roussel[1,2,]*

*Correspondence should be addressed to CC (cambillau@afmb.univ-mrs.fr) or AR (alain.roussel@afmb.univ-mrs.fr)

This PDF file includes:

Supplementary Figures 1-5

Supplementary Tables 1-3
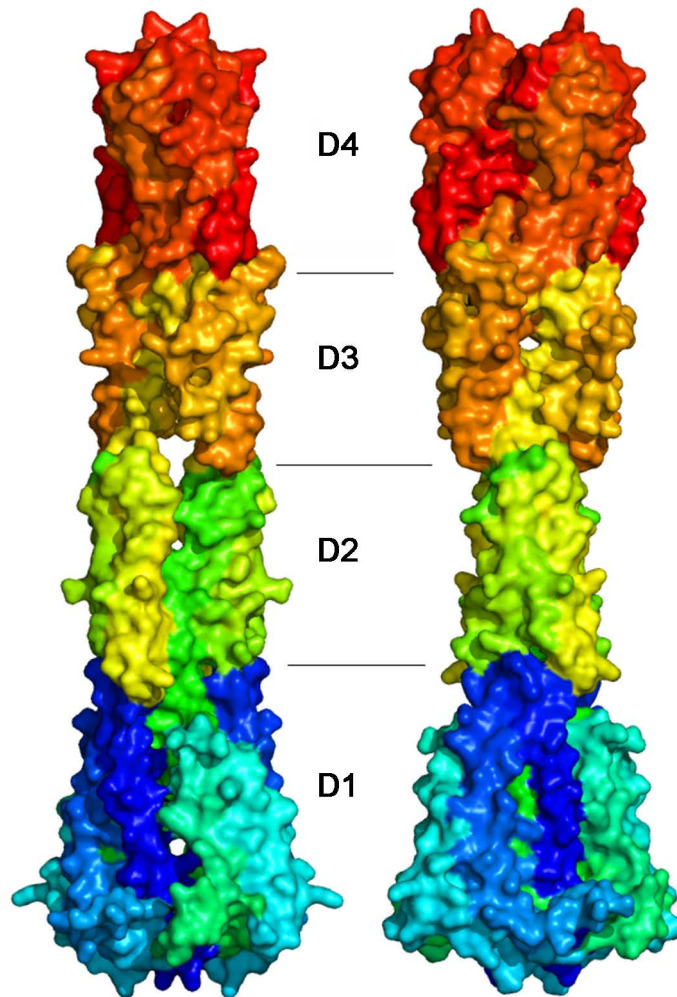
Supplementary Figure 1. Crystal structure of *Flavobacterium johnsonia* GldMp. Surface representation of GldM in two orientations at 90° from each other, around the vertical 2D axis. The colouring is in rainbow mode, from N-terminus (blue) to C-terminus (red). The four domains are numbered D1-4 from N- to C-terminus.
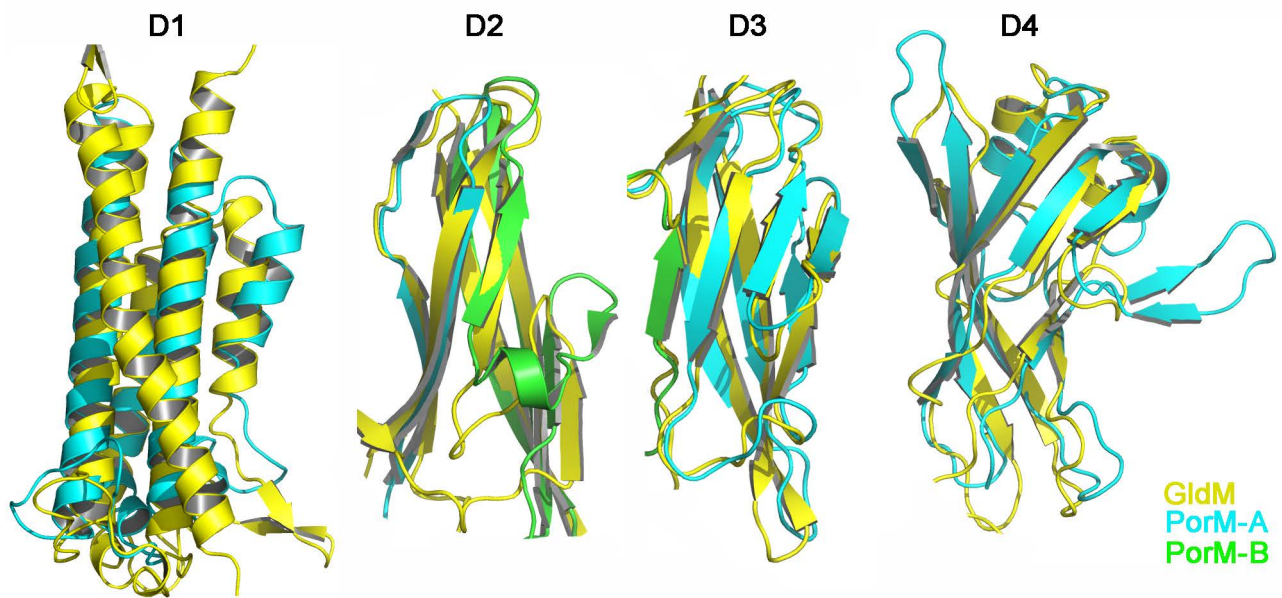
Supplementary Figure 2. Comparison of the four domains of GldMp with those of PorMp. The four domains are numbered D1-4 from N- to C-terminus. GldM domains are coloured yellow, those of PorM monomer A are colored blue. Domain swapping has been evidenced only in PorM, in which monomer B contribution to each domain is colored green.

GldM D2/D3   PorM D2/D3

D3

D2
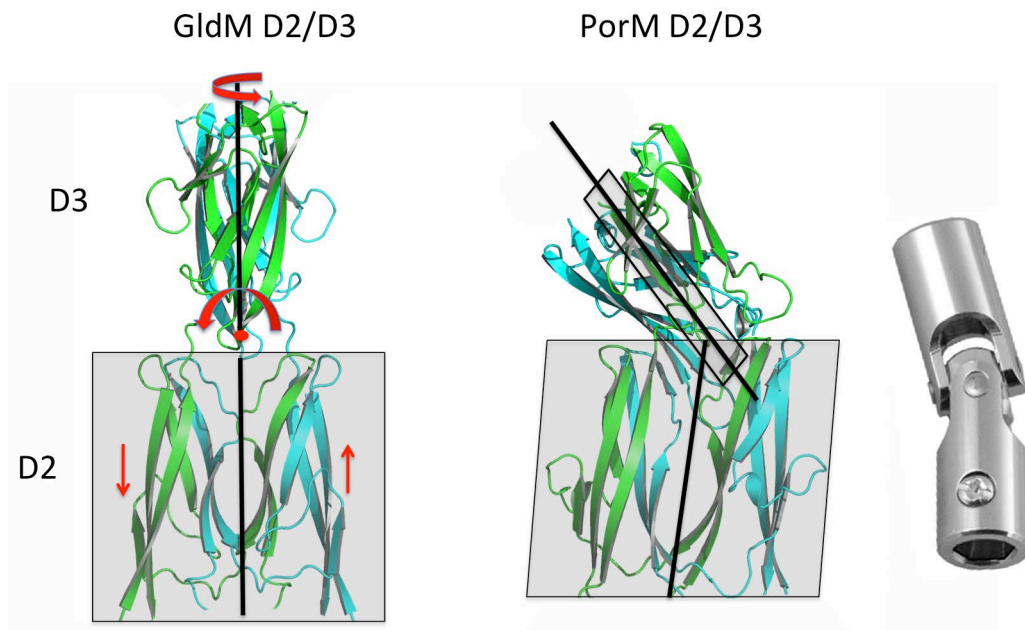
Supplementary Figure 3. Comparison of the association of domains D2 and D3 of GldM with those of PorM. Monomers A and B are coloured blue and green, respectively. The translation/rotation movements that occur to obtain the PorM D2/D3 arrangement are shown by red arrows on GldM. A view of a cardan illustrates the concept of the observed differences between GldM and PorM D2/D3 topology.
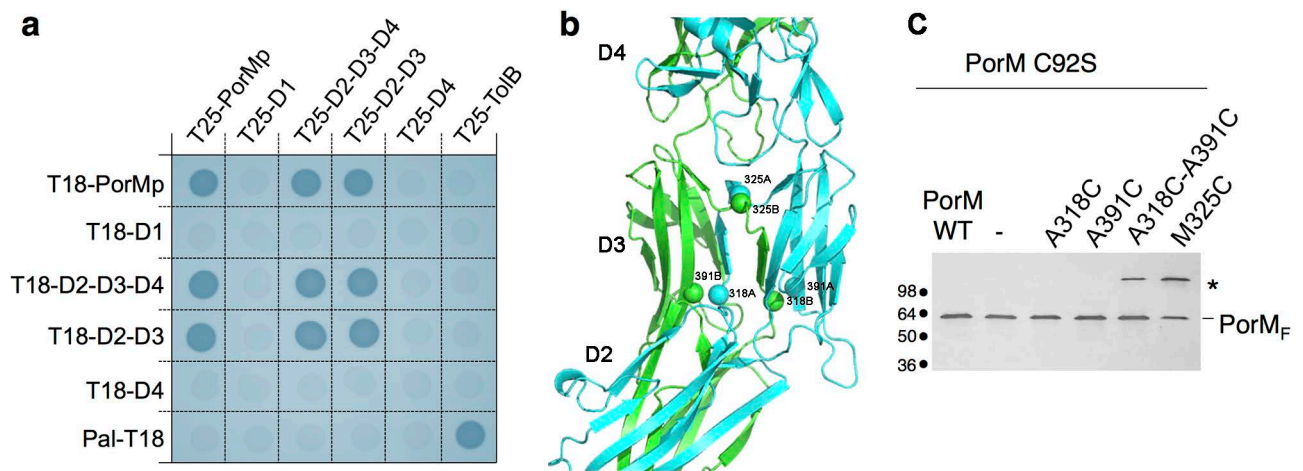
Supplementary Figure 4. *In vivo* **validation of the PorMp structure. a,** Bacterial two-hybrid analysis. BTH101 reporter cells carrying pairs of plasmids producing the indicated PorM fragments fused to the T18 or T25 domain of the *Bordetella* adenylate cyclase were spotted on X-Gal-IPTG reporter LB agar plates. The blue coloration of the colony reports interaction between the two partners. Controls include T18 and T25 fusions to TolB and Pal, two proteins that interact but unrelated to the T9SS. **b,** Ribbon representation of a portion of PorM with the Cys mutants (tested in **c**) identified by spheres. **c,** Disulphide-bond formation. Total membrane fractions from cells producing the wild-type (WT) FLAG-tagged PorM protein, and the indicated cysteine variants introduced into the cysteine-less C92S PorM, were subjected to 10%-acrylamide SDS-PAGE and immunodetected using the anti-FLAG antibody. The asterisk on right indicates bands corresponding to a PorM dimer. Molecular weight markers are shown on right.
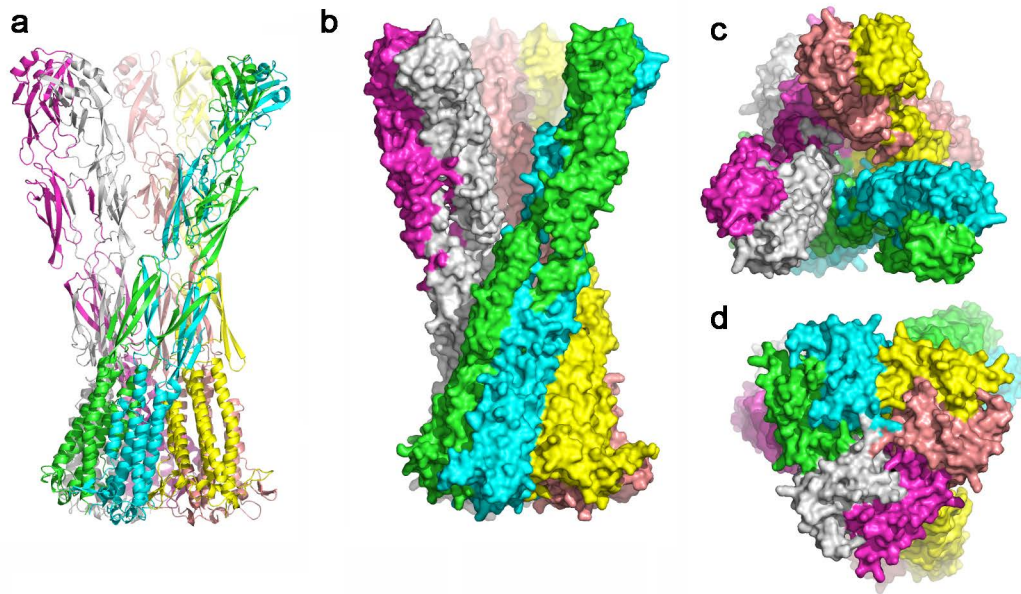
Supplementary Figure 5. Model of an arrangemment of *Flavobacterium johnsonia GldMp* dimer with 3 fold symmetry. a, ribbon representation of the three dimers, the six monomer being coloured individually. **b**, same view as in a, but with surface representation. **c**, same as in b, viewed from top. **d**, same as in b, viewed from bottom.

Supplementary Table 1: Data collection and refinement statistics

	GldMp		PorMp$_{224}$	PorMp$_{315}$/nb130	PorM$_{Nt}$/nb01
Data collection	Se peak	Native			
PDB accession code	na	XXX	XXX	XXX	XXX
Diffraction source	Proxima-1, SOLEIL	ID30A-3, ESRF	ID23-1, ESRF	Proxima-1, SOLEIL	Proxima-1, SOLEIL
Space group	P6$_4$22	P6$_4$22	P4$_3$2$_1$2	P1	P2$_1$
a, b, c (Å)	71.40, 71.40, 426.09	71.37, 71.37, 426.94	77.0, 77.0, 228.56	55.24, 77.18, 156.30	80.35, 100.12, 80.41
α, β, γ (°)	90, 90, 120	90, 90, 120	90, 90, 90	90.24, 91.75, 97.16	90, 93.82, 90
Resolution (Å)[a]	47.34-2.4 (2.53-2.4)	46.66-2.0 (2.11-2.0)	40-2.85 (3.0-2.85)	40-2.1 (2.21-2.1)	42.47-2.4 (2.53-2.4)
Unique reflections[a]	26760 (3769)	45389 (6440)	16929 (2392)	145898 (21179)	49059 (7020)
Multiplicity[a]	20.4 (21.7)	13.6 (14.4)	8.0 (8.0)	2.9 (2.9)	6.9 (6.8)
Completeness (%)[a]	100.0 (99.9)	100.0 (100.0)	99.9 (100.0)	97.6 (96.8)	98.3 (96.7)
I/σ[a]	13.6 (0.9)	10.1 (1.2)	14.8 (2.2)	12.5 (2.0)	11.6 (1.0)
R$_{meas}$ (%)[a,b]	15.3 (335.6)	12.5 (266.0)	8.1 (81.5)	6.5 (76.4)	7.8 (203.3)
R$_{p.i.m.}$ (%)[a,c]	4.5 (97.6)	3.4 (69.4)	2.7 (27.6)	3.7 (43.3)	3.0 (77.4)
CC1/2 [d]	0.999 (0.651)	0.995 (0.667)	0.999 (0.854)	0.998 (0.647)	0.999 (0.755)
Mosaicity	0.13	0.06	0.06	0.19	0.05
Solvent content (%)	55.8	55.9	52.2	43.1	43.4
Refinement and model quality					
Resolution (Å)		43.42-2.0	39.42-2.85	38.35-2.1	40-2.4
Reflections		45244	16861	145522	48833
R$_{cryst}$/R$_{free}$ (%)[e]		21.8/25.8	21.7/24.9	18.0/21.5	21.0/23.9
Number of atoms					
Protein (chain(s) in AU)		3536 (1)	4469 (2)	20169 (16)	8569 (8)
Water/ion/ligand		295/-/32	60/4/-	1236/-/-	159/-/-
Average B-factors (Å^2)Protein/ Water/ion/ligand		69.7/69.2/-/85.8	109.5/78.2/167.1/-	53.4/50.6/-/-	109.4/90.5/-/-
Rmsd[f] Bond (Å) / Angle		0.01 / 1.25	0.01 / 1.23	0.01/1.13	0.09 / 1.11
Ramachandran: most favored/ additionally allowed regions / outliers(%)		95.8 / 2.5 / 1.7	96.2 / 2.9 / 0.9	97.0 / 2.1 /0.9	95.6 / 3.9 / 0.5

[a] Values in parentheses are for the highest-resolution shell. [b] $R_{meas} = \Sigma \sqrt{(n/n-1)} | I_{hl} - <I_h> | / \Sigma | <I_h> |$, where I_{hl} is the observed intensity and $<I_h>$ the average intensity from n observations (symmetry-related and duplicate measurements of a unique reflection). [c] $R_{p.i.m.} = \Sigma \sqrt{(1/n-1)} | I_{hl} - <I_h> | / \Sigma | <I_h> |$. [d] CC$_{1/2}$ values are the half-set correlation coefficients (Karplus & Diederichs, 2012). [e] $R_{cryst}=\Sigma_{hkl}||Fo| - |Fc||/\Sigma_{hkl}|Fo|$; R$_{free}$ is calculated for 5% of randomly selected reflections excluded from refinement. [f] Root mean square deviation from ideal values.

Supplementary Table 2: Hydrogen and ionic bonds established between GldM monomers

Hydrogen Bonds

Monomer 1	distance(Å)	Monomer 2
A:LYS 42[NZ]	3.79	B:LYS 171[O]
A:LYS 160[NZ]	3.32	B:ASN 220[OD1]
A:LYS 170[NZ]	3.47	B:SER 49[OG]
A:LYS 180[NZ]	3.61	B:GLU 116[OE1]
A:SER 232[OG]	2.65	B:GLU 304[OE1]
A:TYR 233[N]	3.16	B:GLU 304[OE2]
A:TYR 236[OH]	2.76	B:TYR 236[OH]
A:ASN 245[ND2]	3.42	B:LYS 316[O]
A:ASN 245[ND2]	3.20	B:ASP 243[O]
A:TYR 247[N]	2.79	B:VAL 318[O]
A:GLY 250[N]	2.79	B:ALA 288[O]
A:VAL 253[N]	2.67	B:LEU 286[O]
A:GLY 255[N]	3.12	B:ILE 284[O]
A:LYS 256[NZ]	2.81	B:GLN 281[OE1]
A:LYS 256[NZ]	3.21	B:GLN 237[OE1]
A:VAL 257[N]	2.92	B:ALA 282[O]
A:ARG 261[N]	2.96	B:LEU 259[O]
A:ARG 261[NH1]	2.95	B:TYR 236[OH]
A:ALA 282[N]	3.32	B:VAL 257[O]
A:ILE 284[N]	2.81	B:GLY 255[O]
A:SER 285[OG]	3.82	B:VAL 253[O]
A:LEU 286[N]	3.27	B:VAL 253[O]
A:ALA 288[N]	2.78	B:GLU 251[O]
A:VAL 318[N]	2.80	B:ASN 245[O]
A:VAL 320[N]	2.89	B:TYR 247[O]
A:ARG 322[NE]	2.79	B:ASP 394[OD2]
A:ARG 322[NH1]	2.82	B:GLN 249[O]
A:ARG 322[NH2]	2.84	B:ASP 394[OD2]
A:ARG 322[NH2]	3.05	B:GLN 249[O]
A:ALA 326[N]	2.76	B:ASP 398[OD2]
A:THR 327[N]	2.78	B:SER 347[O]
A:THR 327[OG1]	2.79	B:THR 327[OG1]
A:SER 329[N]	2.85	B:SER 345[O]
A:ASP 331[N]	2.94	B:PRO 343[O]
A:LYS 332[NZ]	2.82	B:ASP 441[O]
A:SER 345[N]	2.76	B:SER 329[O]
A:SER 345[N]	3.41	B:ASP 331[OD1]
A:SER 345[OG]	2.73	B:ASP 331[OD1]
A:SER 347[N]	2.95	B:THR 327[O]
A:SER 347[OG]	3.81	B:THR 327[O]
A:LYS 400[NZ]	2.91	B:ILE 328[O]
A:ARG 403[NH1]	3.05	B:ASP 441[OD2]
A:ARG 403[NH2]	3.19	B:ASP 441[OD2]
A:LYS 405[NZ]	2.77	B:ASP 441[OD2]
A:LYS 405[NZ]	2.77	B:ASP 439[O]
A:THR 486[OG1]	2.67	B:GLN 484[OE1]
A:SER 49[OG]	3.47	B:LYS 170[NZ]
A:GLU 116[OE1]	3.61	B:LYS 180[NZ]
A:LYS 171[O]	3.79	B:LYS 42[NZ]
A:ASN 220[OD1]	3.32	B:LYS 160[NZ]
A:TYR 236[OH]	2.95	B:ARG 261[NH1]
A:GLN 237[OE1]	3.21	B:LYS 256[NZ]
A:ASP 243[O]	3.20	B:ASN 245[ND2]
A:ASN 245[O]	2.80	B:VAL 318[N]
A:TYR 247[O]	2.89	B:VAL 320[N]
A:GLN 249[O]	2.82	B:ARG 322[NH1]
A:GLN 249[O]	3.05	B:ARG 322[NH2]
A:GLU 251[O]	2.78	B:ALA 288[N]
A:VAL 253[O]	3.82	B:SER 285[OG]
A:VAL 253[O]	3.27	B:LEU 286[N]
A:GLY 255[O]	2.81	B:ILE 284[N]
A:VAL 257[O]	3.32	B:ALA 282[N]
A:LEU 259[O]	2.96	B:ARG 261[N]
A:GLN 281[OE1]	2.81	B:LYS 256[NZ]
A:ALA 282[O]	2.92	B:VAL 257[N]
A:ILE 284[O]	3.12	B:GLY 255[N]
A:LEU 286[O]	2.67	B:VAL 253[N]
A:ALA 288[O]	2.79	B:GLY 250[N]
A:GLU 304[OE1]	2.65	B:SER 232[OG]
A:GLU 304[OE2]	3.16	B:TYR 233[N]
A:LYS 316[O]	3.42	B:ASN 245[ND2]
A:VAL 318[O]	2.79	B:TYR 247[N]
A:THR 327[O]	3.81	B:SER 347[OG]
A:THR 327[O]	2.95	B:SER 347[N]
A:ILE 328[O]	2.91	B:LYS 400[NZ]
A:SER 329[O]	2.76	B:SER 345[N]
A:ASP 331[OD1]	2.73	B:SER 345[OG]
A:ASP 331[OD1]	3.41	B:SER 345[N]
A:PRO 343[O]	2.94	B:ASP 331[N]
A:SER 345[O]	2.85	B:SER 329[N]
A:SER 347[O]	2.78	B:THR 327[N]
A:ASP 394[OD2]	2.79	B:ARG 322[NE]
A:ASP 394[OD2]	2.84	B:ARG 322[NH2]
A:ASP 398[OD2]	2.76	B:ALA 326[N]
A:ASP 439[O]	2.77	B:LYS 405[NZ]
A:ASP 441[OD2]	2.77	B:LYS 405[NZ]
A:ASP 441[OD2]	3.05	B:ARG 403[NH1]
A:ASP 441[OD2]	3.19	B:ARG 403[NH2]
A:ASP 441[O]	2.82	B:LYS 332[NZ]
A:GLN 484[OE1]	2.67	B:THR 486[OG1]

Ionic bonds

Monomer 1	distance(Å)	Monomer 2
A:LYS 42[NZ]	3.37	B:ASP 210[OD2]
A:LYS 180[NZ]	3.61	B:GLU 116[OE1]
A:ARG 322[NE]	2.79	B:ASP 394[OD2]
A:ARG 322[NH2]	2.84	B:ASP 394[OD2]
A:ARG 403[NH1]	3.41	B:ASP 441[OD1]
A:ARG 403[NH1]	3.05	B:ASP 441[OD2]
A:ARG 403[NH2]	3.19	B:ASP 441[OD2]
A:LYS 405[NZ]	3.26	B:ASP 441[OD1]
A:LYS 405[NZ]	2.77	B:ASP 441[OD2]
A:GLU 116[OE1]	3.61	B:LYS 180[NZ]
A:ASP 210[OD2]	3.37	B:LYS 42[NZ]
A:ASP 394[OD2]	2.79	B:ARG 322[NE]
A:ASP 394[OD2]	2.84	B:ARG 322[NH2]
A:ASP 441[OD1]	3.26	B:LYS 405[NZ]
A:ASP 441[OD1]	3.41	B:ARG 403[NH1]
A:ASP 441[OD2]	2.77	B:LYS 405[NZ]
A:ASP 441[OD2]	3.05	B:ARG 403[NH1]
A:ASP 441[OD2]	3.19	B:ARG 403[NH2]

Supplementary Table 3: Structural comparison of GldM and PorM domains.

Domain (monomer)	Residues in domain	Residues aligned (%)	Rmsd (Å)
D1 (α1 missing)	143	124 (86)	3.5
D2 (A+B swapped)	89	74 (83)	1.7
D3 (A+B swapped)	100	89 (89)	1.6
D4	117	104 (89)	2.15